


An Investigation on the Applicability of the Integrated Method for Multi-Carrier Energy Flow Analysis

Conference Paper**Author(s):**

[Jia, Mengshuo](#) ; Shaowei, Huang; Tang, Kexuan; Shen, Chen

Publication date:

2018

Permanent link:

<https://doi.org/10.3929/ethz-b-000526363>

Rights / license:

[In Copyright - Non-Commercial Use Permitted](#)

Originally published in:

<https://doi.org/10.1109/PESGM.2018.8585831>

An Investigation on the Applicability of the Integrated Method for Multi-Carrier Energy Flow Analysis

Mengshuo Jia, Shaowei Huang, Kexuan Tang, Chen Shen

State Key Lab of Power Systems
Department of Electrical Engineering
Tsinghua University
Beijing, China

Abstract—The integrated energy system (IES) combined with electricity and heat networks is a research hotspot in energy field in recent years. As the foundation of security and economy analysis of IES, the steady-state multi-carrier energy flow (MEF) analysis is important but difficult to converge. An integrated method for solving MEF has been presented and adopted in some published literatures. In this paper, we investigate the integrated method and point out its two problems: one is the failure of the integrated method when energy reverses during iteration in some exceptional cases; the other is the high sensitivity of the method to the initial value. Thereafter, the fundamental causes for the two problems are revealed. Moreover, we modify the integrated method based on the fundamental causes to deal with the two problems. The cost and benefit of the modified integrated method are analyzed as well. Finally, the integrated method and the modified integrated method are discussed on the basis of theoretical and simulation results. The results show that with fewer iteration times and less calculation time, the modified integrated method has better applicability to exceptional cases and less sensitivity to the initial value.

Index Terms—Integrated energy system, multi-carrier energy flow analysis, Combined Heat and Power, integrated method.

I. INTRODUCTION

Recently the development of integrated energy system becomes an important trend in energy field. The increasing utilization of cogeneration plants continuously enhances the energy efficiency as well as the consumption of renewable energy, and strengthens the interdependence of multi-carrier energies.

Aiming at improving the energy efficiency, increasing renewable energy consumption and reducing pollution emission, the corresponding research on IES mainly focuses on optimal multi-carrier energy flow analysis [1], optimal multi-carrier energy dispatch [2] and optimal planning based on energy hub [3]. Being the foundation of the above mentioned research, steady-state multi-carrier energy flow (MEF) analysis is important for investment planning and operation decision.

The MEF analysis of IES is still facing many problems, being difficult to converge is the most important one. Some efforts have already been made in related field, and the state-of-the-art achievement can be divided into two aspects: one is the

decomposed MEF method [4]-[6], which calculates energy flow for each network independently and combines the calculation results through alternate iteration; the other is the integrated MEF method, which formulates the unified framework of IES combined with electricity, heat network or gas network and calculates MEF as a whole [6]-[10]. Due to the passively alternate iteration, the convergence of the decomposed method is inferior to the integrated method [10]. Thus the integrated method is favored by many researchers and becomes common in relevant research [11]-[13].

However, we found two problems of the integrated method: one is the failure of the integrated method in some exceptional cases; the other is the high sensitivity of the method to the initial value. Therefore, based on the IES combined with the electricity and heat network, this paper focuses on investigating the applicability of the integrated method and modifying it. Main contributions of this paper are threefold:

- The two problems of the integrated method are demonstrated. Thereafter, the fundamental causes for the two problems of the integrated method are revealed.
- The integrated method is modified to deal with the two problems. The modified integrated method shows better applicability to exceptional cases and less sensitivity to the initial value.
- The cost and benefit of the modified integrated method are analyzed by comparing with the integrated method. The modified integrated method needs fewer iteration times and less calculation time.

The remainder of this paper is organized as follows: Section II introduces the integrated method. Section III investigates the applicability of the integrated method, details the problems of the integrated method and reveals the fundamental causes for the problems. Thereafter, the integrated method is modified in section IV. The cost and benefit analysis of the modifications are demonstrated as well. Case studies are performed in Section V to compare the modified integrated method with the integrated method. Finally, Section VI concludes this paper.

II. THE INTEGRATED METHOD

Combined with electricity and district heat network, the IES model consists of the electricity network model, the district heat

network model (including the hydraulic part and the thermal part) and coupling components model. In the integrated method, the electrical power flow equations, the hydraulic equations and some of the thermal equations were combined and solved simultaneously by using Newton-Raphson iterative calculation, and the rest equations are solved separately[6].

A. IES Model

The electricity network model is given in (1); the hydraulic model is given in (2)-(4); the thermal model is given in (5)-(7); the coupling components model is given in (8)-(10). Detailed descriptions are available in [6], [10]-[11].

$$\begin{cases} P_i^{SP} = V_i \sum_{j \in i} V_j (G_{ij} \cos \theta_{ij} + B_{ij} \sin \theta_{ij}) \\ Q_i^{SP} = V_i \sum_{j \in i} V_j (G_{ij} \sin \theta_{ij} - B_{ij} \cos \theta_{ij}) \end{cases} \quad (1)$$

$$\mathbf{A}\dot{\mathbf{m}} = \dot{\mathbf{m}}_q \quad (2)$$

$$\mathbf{B}\mathbf{h} = 0 \quad (3)$$

$$\mathbf{h} = \mathbf{k}\dot{\mathbf{m}}|\dot{\mathbf{m}}| \quad (4)$$

$$\begin{cases} \Phi_{load}^{SP} = C_p \dot{m}_q (T_{s,load} - T_{0,load}) \\ \Phi_{source}^{SP} = C_p \dot{m}_q (T_{s,source} - T_{r,source}) \end{cases} \quad (5)$$

$$T^{end} = (T^{start} - T_a) e^{-\frac{\lambda_i L_i}{C_p \dot{m}_i}} + T_a \quad (6)$$

$$(\sum \dot{m}_{out}) T_{out} = \sum (\dot{m}_{in} T_{in}) \quad (7)$$

$$\Phi_{CHP} = C_m P_{CHP} \quad (8)$$

$$P_{CHP} = C_p \mathbf{A}_{slack} \dot{\mathbf{m}} (T_{s,slack} - T_{r,slack}) C_m^{-1} \quad (9)$$

$$\Phi_{CHP} = Real[V_{slack} \sum_{j=1}^N (\bar{Y}_{slack,j} \bar{V}_j)] C_m \quad (10)$$

For brief, the temperature of nodes, say, $\mathbf{T}_s = [\mathbf{T}_{s,source}, \mathbf{T}_{s,load}]$, $\mathbf{T}_r = [\mathbf{T}_{r,source}, \mathbf{T}_{r,load}]$ and $\mathbf{T}_{0,load}$ are denoted by $\mathbf{T}_{sa} = [\mathbf{T}_{sa,source}, \mathbf{T}_{sa,load}]$, $\mathbf{T}_{ra} = [\mathbf{T}_{ra,source}, \mathbf{T}_{ra,load}]$ and $\mathbf{T}_{0a,load}$ via (11):

$$\begin{cases} \mathbf{T}_{sa} = \mathbf{T}_s - \mathbf{T}_a \\ \mathbf{T}_{ra} = \mathbf{T}_r - \mathbf{T}_a \\ \mathbf{T}_{0a,load} = \mathbf{T}_{0,load} - \mathbf{T}_a \end{cases} \quad (11)$$

where \mathbf{T}_a is the ambient temperature.

B. The Integrated Method

The Newton-Raphson iteration is part of the integrated method. The corresponding iterative form is given in (12).

$$\mathbf{x}^{(k+1)} = \mathbf{x}^{(k)} - \mathbf{J}(k) \Delta \mathbf{F}(k) \quad (12)$$

where $\Delta \mathbf{F}$ is the deviation shown in (13), among which $\Delta \Phi$ is corresponding to (2), (5), (8) and (10), $\Delta \mathbf{h}$ is corresponding to (3) and (4), $\Delta \mathbf{P}$ and $\Delta \mathbf{Q}$ is corresponding to (1), (8) and (9). And based on (6)-(7), $\Delta \mathbf{T}_{sf}$ is calculated via (14) and $\Delta \mathbf{T}_{rf}$ is calculated via (15), where the high corner mark 'load' and 'source' represent the type of the starting node for $\dot{\mathbf{m}}$.

$$\Delta \mathbf{F} = [\Delta \Phi \quad \Delta \mathbf{h} \quad \Delta \mathbf{T}_{sf} \quad \Delta \mathbf{T}_{rf} \quad \Delta \mathbf{P} \quad \Delta \mathbf{Q}] \quad (13)$$

$$\Delta \mathbf{T}_{sf} = (\sum \dot{m}_{out}) T_{sa,load}^{start} - \sum (\dot{m}_m^{load} T_{sa,load}^{end} + \dot{m}_m^{source} T_{sa,source}^{end}) \quad (14)$$

$$\Delta \mathbf{T}_{rf} = (\sum \dot{m}_{out}) T_{ra,load}^{start} - \sum (\dot{m}_m^{load} T_{ra,load}^{end} + \dot{m}_q T_{0a,load}^{end}) \quad (15)$$

Besides, in (12), \mathbf{x} is the unknown variables as shown in (16); \mathbf{J} is the Jacobian matrix as shown in (17), where $\Delta \mathbf{Z} = [\Delta \Phi; \Delta \mathbf{h}]$, $\Delta \mathbf{T} = [\Delta \mathbf{T}_{sf}; \Delta \mathbf{T}_{rf}]$, $\mathbf{T} = [\mathbf{T}_s; \mathbf{T}_r]$; k is the k th iteration.

$$\mathbf{x} = [\dot{\mathbf{m}} \quad \mathbf{T}_{sa,load} \quad \mathbf{T}_{ra,load} \quad \boldsymbol{\theta} \quad \mathbf{V}] \quad (16)$$

$$\mathbf{J} = \begin{bmatrix} \mathbf{J}_h & \mathbf{J}_{he} \\ \mathbf{J}_{eh} & \mathbf{J}_e \end{bmatrix} = \begin{bmatrix} \frac{\partial \Delta \mathbf{Z}}{\partial \dot{\mathbf{m}}} & \frac{\partial \Delta \mathbf{Z}}{\partial \mathbf{T}} & \frac{\partial \Delta \mathbf{Z}}{\partial \boldsymbol{\theta}} & \frac{\partial \Delta \mathbf{Z}}{\partial \mathbf{V}} \\ \frac{\partial \Delta \mathbf{T}}{\partial \dot{\mathbf{m}}} & \frac{\partial \Delta \mathbf{T}}{\partial \mathbf{T}} & 0 & 0 \\ \frac{\partial \Delta \mathbf{P}}{\partial \dot{\mathbf{m}}} & \frac{\partial \Delta \mathbf{P}}{\partial \mathbf{T}} & \frac{\partial \Delta \mathbf{P}}{\partial \boldsymbol{\theta}} & \frac{\partial \Delta \mathbf{P}}{\partial \mathbf{V}} \\ \frac{\partial \Delta \mathbf{Q}}{\partial \dot{\mathbf{m}}} & \frac{\partial \Delta \mathbf{Q}}{\partial \mathbf{T}} & \frac{\partial \Delta \mathbf{Q}}{\partial \boldsymbol{\theta}} & \frac{\partial \Delta \mathbf{Q}}{\partial \mathbf{V}} \end{bmatrix} \quad (17)$$

After each Newton-Raphson iteration according to (12), $\mathbf{T}_{ra,source}$ is calculated by the updated $\mathbf{T}_{ra,load}$ and $\dot{\mathbf{m}}$ via (18):

$$(\sum \dot{m}_{out}) T_{ra,source}^{start} = \sum (\dot{m}_m T_{ra,load}^{end}) \quad (18)$$

Thereafter, the updated $\mathbf{T}_{ra,source}$ is input into (12) as parameters according to (5) and (9). Thus (12) and (18) are solved alternately in the integrated method.

For brief, the alternately solving of (12) and (18) is called 'separate calculation of $\mathbf{T}_{ra,source}$ ' in the following part of this paper.

III. THE APPLICABILITY OF THE INTEGRATED METHOD

Through the investigation of the integrated method, we point out the two problems of the method and reveal the corresponding fundamental causes.

A. Problem One: The Failure of The Integrated Method in Exceptional Cases

1) Problem Description

The integrated method will fail during the iterative calculation when one of the two cases occurs:

- The initial value of electrical variables cause the power injected at the slack bus being negative, which result in a negative Φ at the source node in heat network.
- The initial value of $\dot{\mathbf{m}}$ is far from the convergent solution, which is very normal because the choice of initial value of MEF is not as intuitive as those of electricity network.

2) Fundamental Cause Of The Failure

In the integrated method, due to the separate calculation, $\mathbf{T}_{ra,source}$ is not involved in the Newton-Raphson iteration as variables, but as parameters. However, (15) is equal to zero only under the condition that one $T_{ra,load}$ can only be determined by other $T_{ra,load}$ and $T_{0a,load}$. This condition holds only when energy flows from source nodes to loads, or from load nodes to load nodes, as illustrated in Fig. 1. In the scenarios where the condition holds, the integrated method with separate calculation of $\mathbf{T}_{ra,source}$ works well.

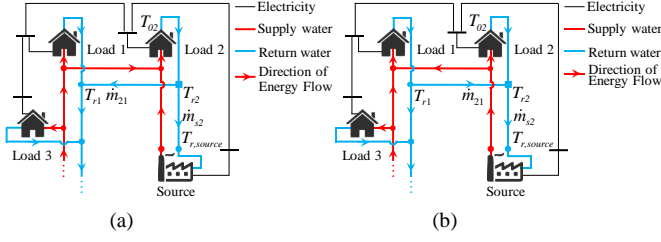


Figure 1. Different direction of mass flow rate between node 1 and 2
(a) scenario 1 ; (b) scenario 2.

In fact, considering the direction of energy in the reality, the condition holds naturally. However, when the two exceptional cases mentioned above occur, it is possible that energy reverses and flows from load nodes to source nodes during iterative calculation, as illustrated in Fig. 2.

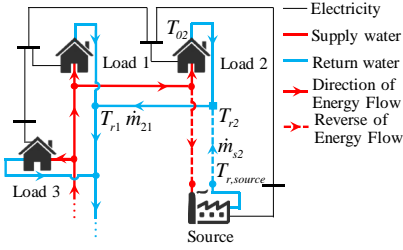


Figure 2. The reverse of energy flow in IES during iteration

In these exceptional cases, $T_{ra,load}$, say, T_{ra2} , is determined by $T_{ra,source}$ as given in (19). Thereafter the condition for the separate calculation of $\mathbf{T}_{ra,source}$ is untenable and the integrated method fails.

$$\dot{m}_{21}T_{ra2} = (\dot{m}_{21} - \dot{m}_{s2})T_{0a2} + \dot{m}_{s2}T_{ra,source} e^{\frac{\lambda_{s2}L_{s2}}{C_p\dot{m}_{s2}}} \quad (19)$$

B. Problem Two: The high Sensitivity Of The Integrated Method To Initial Value

1) Problem Description

The integrated method is highly sensitive to the initial value. Since the initial values of MEF is not as intuitive as those of the electricity network, the convergence of the integrated method is not satisfying.

2) Fundamental Cause Of The Problem

In the integrated method, as the non-diagonal elements of Jacobian matrix, $\partial\Delta\mathbf{T}/\partial\dot{\mathbf{m}}$ is ignored and set as zero. However, $\partial\Delta\mathbf{T}/\partial\dot{\mathbf{m}}$ can be set as zero only when the absolute values of its elements are much smaller than those of the diagonal elements. But the condition may not be tenable in some situations. When the condition is not tenable, setting $\partial\Delta\mathbf{T}/\partial\dot{\mathbf{m}}$ as zero will greatly affect the convergent direction of the integrated method.

Consider $\partial\Delta\mathbf{T}_{sf}/\partial\dot{\mathbf{m}}$ in Fig. 3 at load node i ($\partial\Delta\mathbf{T}_{rf}/\partial\dot{\mathbf{m}}$ is similar). The ratio of the absolute value of $\partial\Delta\mathbf{T}_{sf}/\partial\dot{\mathbf{m}}$ to its corresponding diagonal element is given in (20). According to [6], the range of $\dot{\mathbf{m}}$ in district heat network is from 0.1 to 5 kg/s. But the range of temperature in supply network is from 97.7°C to 99.1°C. Therefore, consider $\dot{\mathbf{m}}$ as variables and set

T_{si} as the middle value of its range. Meanwhile, based on the range of $\dot{\mathbf{m}}$, the upper bound value of the diagonal element in (20) is denoted in (21).

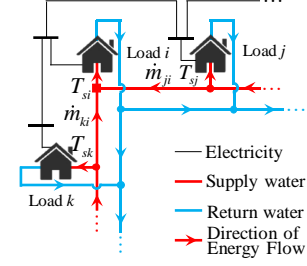


Figure 3. A general scenario in supply water network

$$\left| \frac{\partial\Delta T_{si}}{\partial\dot{m}_{ji}} \right| = \left| T_{si} - T_{sj} e^{\frac{\lambda_{ji}L_{ji}}{C_p\dot{m}_{ji}}} - \frac{\lambda_{ji}L_{ji}}{C_p} T_{sj} e^{\frac{\lambda_{ji}L_{ji}}{C_p\dot{m}_{ji}}} \dot{m}_{ji}^{-1} \right| \quad (20)$$

$$\left| \sum_{j \neq i} \dot{m}_{ji} \right| = \sum_{j \neq i} \dot{m}_{ji} \quad (21)$$

$$\left| \sum_{j \neq i} \dot{m}_{ji} \right|^{upper} = \dot{m}_{ji} + \sum \dot{m}_{ji}^{upper} = \dot{m}_{ji} + 5 + \dots + 5$$

Replace the diagonal element in (20) by its upper bound value and re-calculate the ratio. The result is given in Fig. 4.

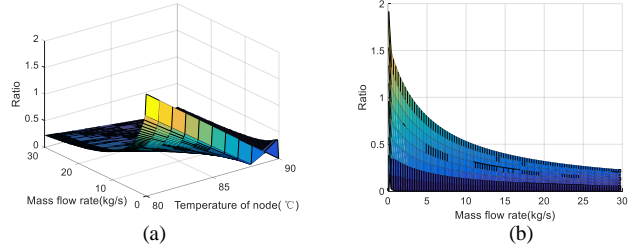


Figure 4. The ratio of absolute value
(a) Original view ; (b) Ratio-mass flow rate view.

As shown in Fig. 4(b), with the increase of $\dot{\mathbf{m}}$, the ratio decreases to 0, which means that the condition of zero setting holds. However, even if the diagonal element is replaced by its upper bound value, the ratio will still reach to 0.8 and above when $\dot{\mathbf{m}}$ varies under 5 kg/s. Thus, when the $\dot{\mathbf{m}}$ is under 5kg/s, the condition is untenable. It is important to note that, [0.1, 5] is the most common range of $\dot{\mathbf{m}}$ according to [6]. Therefore, normally speaking, the condition of setting $\partial\Delta\mathbf{T}/\partial\dot{\mathbf{m}}$ as zero is untenable, and the convergence of the integrated method is deteriorated, which lead to the high sensitivity to the initial value.

IV. THE MODIFICATIONS OF THE INTEGRATED METHOD

To overcome the two problems of the integrated method, we make two corresponding modifications. Moreover, we analyze the cost and benefit of the modifications qualitatively.

A. The Modifications Of The Integrated Method

The first modification is solving all equations and variables simultaneously in the Newton-Raphson iteration. Since the condition of the separate calculation of $\mathbf{T}_{ra,source}$ is not always

tenable, especially when the exceptional cases occur, thus (18) should be calculated simultaneously in the Newton-Raphson iteration via (22), and $\mathbf{T}_{ra,source}$ should be added into \mathbf{x} via (23):

$$\Delta \mathbf{F} = \begin{bmatrix} \Delta \Phi & \Delta \mathbf{h} & \Delta \mathbf{T}_{sf,load} & \Delta \mathbf{T}_{rf} & \Delta \mathbf{P} & \Delta \mathbf{Q} \end{bmatrix} \quad (22)$$

$$\mathbf{x} = \begin{bmatrix} \dot{\mathbf{m}} & \mathbf{T}_{sa,load} & \mathbf{T}_{ra} & \boldsymbol{\theta} & \mathbf{V} \end{bmatrix} \quad (23)$$

where $\Delta \mathbf{T}_{rf} = [\Delta \mathbf{T}_{rf,load}; \Delta \mathbf{T}_{rf,source}]$, $\mathbf{T}_{ra} = [\mathbf{T}_{ra,load}; \mathbf{T}_{ra,source}]$. And $\Delta \mathbf{T}_{rf}$ is calculated via (24) and (25).

$$\Delta T_{rf,load} = (\sum \dot{m}_{out}) T_{ra,load}^{start} - \sum \begin{bmatrix} \dot{m}_m^{load} & \dot{m}_m^{source} & \dot{m}_q \end{bmatrix} \begin{bmatrix} T_{ra,load}^{end} \\ T_{ra,source}^{end} \\ T_{0a,load} \end{bmatrix} \quad (24)$$

$$\Delta T_{rf,source} = (\sum \dot{m}_{out}) T_{ra,source}^{start} - \sum (\dot{m}_m T_{ra,load}^{end}) \quad (25)$$

The second modification is calculating the Jacobian non-diagonal submatrix considering the range of variables. Based on the most common range of $\dot{\mathbf{m}}$ according to [6], $\partial \Delta \mathbf{T} / \partial \dot{\mathbf{m}}$ in the Jacobian matrix should be calculated exactly.

B. The Cost And Benefit Of The Modifications

As for the cost, the simultaneous calculation of all equations and variables in Newton-Raphson iteration increases the dimension of the Jacobian matrix. Moreover, the exact calculation of the $\partial \Delta \mathbf{T} / \partial \dot{\mathbf{m}}$ increases the number of non-zero elements in the Jacobian matrix. Therefore, the inverse computation burden of the Jacobian matrix is increased in each Newton-Raphson iteration.

As for the benefit, the modifications eliminate the failure when the exceptional cases occur. Moreover, the modifications correct the convergent direction, thus the iteration times are reduced. It's worth noting that, even though the computation burden of each iteration is increased, the iteration times are reduced greatly and the whole computation time is still decreased. The quantitative verification is given in Section V.

V. CASE STUDY

To compare the integrated method and the modified integrated method, simulations on a testing IES is conducted. The schematic diagram of the IES is shown in Fig. 5.

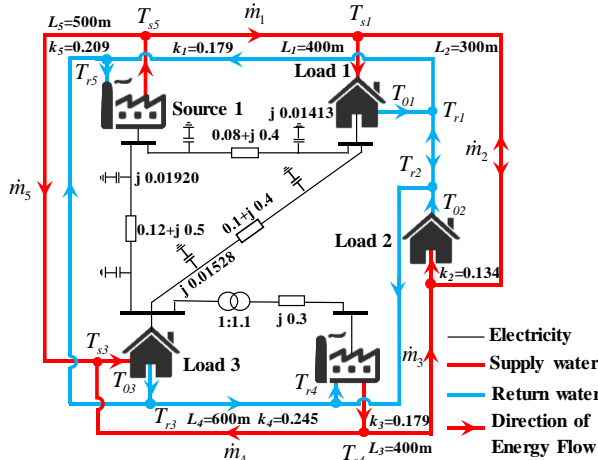


Figure 5. The schematic diagram of the testing IES

The corresponding parameters are given in Table I. It worth noting that when the iteration times reach 100, the calculation is stopped and the case is regarded as divergent.

TABLE I. CASE PARAMETERS OF THE TESTING IES

Type	Parameters Value	Parameters Value
Electricity Network	$P^{sp1} = -0.3\text{MW}$	$P^{sp2} = -0.55\text{MW}$
	$Q^{sp1} = -0.08\text{MVar}$	$Q^{sp2} = -0.1\text{MVar}$
	$V_3 = 1.05 \text{ p.u.}$	$V_4 = 1.05 \text{ p.u.}$
	$\theta_r = 0 \text{ rad}$	
Heat Network	$\Phi^{sp1} = -0.4\text{MW}$	$\Phi^{sp2} = -0.3\text{MW}$
	$\Phi^{sp3} = -0.3\text{MW}$	$\Phi^{sp4} = 0.3\text{MW}$
	$T_a = 10^\circ\text{C}$	$T_0 = 50^\circ\text{C}$
	$C_{mj} = 1/0.79$	$\lambda = 0.236\text{W}/(\text{m}^\circ\text{C})$
	$C_p = 4.182\text{kJ}/(\text{kg}^\circ\text{C})$	$C_{m2} = 1/0.85$
Iteration	$\epsilon = 10^{-5}$	$N_{max} = 100$

A. Applicability Comparison

To expose the failure of the integrated method, 5184 scenarios are chosen based on the initial value set of $\boldsymbol{\theta}$ and $\dot{\mathbf{m}}$.

In Table II, each θ has 4 candidates to choose in its set, and each \dot{m} has 3 candidates. Among these scenarios, both situations which can cause the reverse of energy are included. Both the integrated method and the modified integrated method are used to calculate these scenarios. The computation results are demonstrated in Fig. 6.

TABLE II. INITIAL VALUE SET OF PHASE ANGLE AND MASS FLOW RATE

$\boldsymbol{\theta}$	Initial Value Set	$\dot{\mathbf{m}}$	Initial Value Set
$\theta_1, \theta_2, \theta_3$	$\{-0.1, 0, 0.1, 0.2\}$	$\dot{m}_1, \dot{m}_2, \dot{m}_3, \dot{m}_4$	$\{1, 1.5, 3\}$

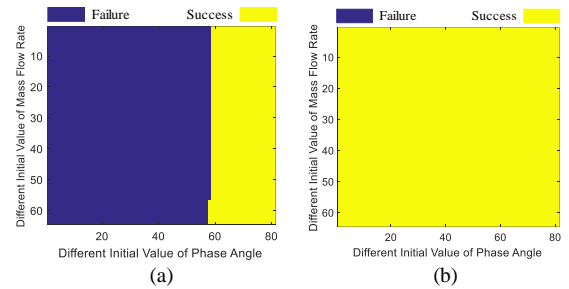


Figure 6. The computation results under different initial value of $\boldsymbol{\theta}$ and $\dot{\mathbf{m}}$
(a) The integrated method ; (b) The modified integrated method.

As shown in Fig. 6, each point represents a scenario with relative initial values. A blue colored point indicates that the method fails in solving the corresponding scenario, and the yellow colored point indicates the success of the method. Failure means the energy reverse occurs and the calculation of the method is terminated. Success means the method can converge or diverge within the 100 iteration times. In Fig. 6(a), the integrated method fails in 71.45% of all the scenarios. But in Fig. 6(b), the modified integrated method can conduct the calculation for all scenarios.

As for the computation efficiency, the scenarios with the top ten iteration times of the integrated method are chosen. The calculating time of this ten scenarios calculated by the two methods are given in Fig. 7. Such results demonstrate that although the integrated method reduces computation burden of each iteration by separately calculating $\mathbf{T}_{ra,source}$ and setting $\partial \Delta \mathbf{T} / \partial \dot{\mathbf{m}}$ as zero, the deteriorated convergence counteracts the simplification effort. Table III gives the comparison results of the two methods for the whole 5184 scenarios.

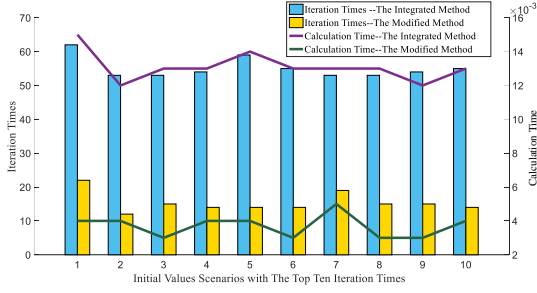


Figure 7. The iteration times and calculating time of the two method in the scenarios with the top ten iteration times of the integrated method

TABLE III. AVERAGE CONVERGENCE CHARACTERISTICS COMPARISON

Comparison	Failure Rate	Average Iteration times	Average Calculation Time
The Integrated Method	71.45%	33.91	8.4×10^{-3} s
The Modified Method	0	17.52	4.4×10^{-3} s
Improvement	100%	48.33%	47.62%

B. Initial Value Sensitivity Comparison

To verify the inference that setting $\partial\Delta T/\partial\dot{m}$ zero when the \dot{m} is under 5 kg/s is improper and will increase the initial value sensitivity and further decrease the convergence, only setting $\partial\Delta T/\partial\dot{m}$ as zero is considered in the integrated method; (12) and (18) are calculated as a whole in the Newton-Raphson iteration.

1024 initial value scenarios are forged according to the initial value set of \dot{m} as shown in Table IV. Each \dot{m} has 4 candidate values.

Fig. 8 shows the convergence results of the two methods. As shown in Fig. 8(a), most of the scenarios are divergent. But in Fig. 8(b), accurate calculation of $\partial\Delta T/\partial\dot{m}$ greatly reduce the divergent situations. Table V gives the comparison results for the two methods for the whole 1024 scenarios.

TABLE IV. INITIAL VALUE SET OF MASS FLOW RATE

\dot{m}	Initial Value Set
$\dot{m}_1, \dot{m}_2, \dot{m}_3, \dot{m}_4, \dot{m}_5$	{1, 1.5, 2, 2.5}

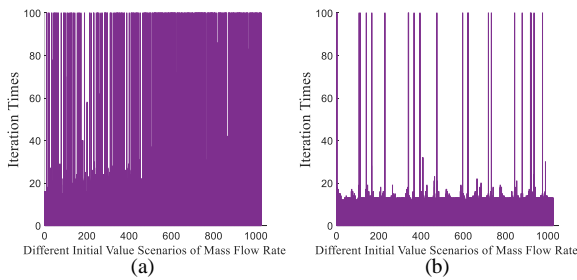


Figure 8. The iteration times under different initial value of mass flow rate (a) The integrated method; (b) The modified integrated method.

TABLE V. INITIAL VALUE SENSITIVITY COMPARISON

Comparison	Divergent Times	Average Iteration times	Average Calculation Time
The Integrated Method	324	21.73	5.9×10^{-3} s
The Modified Method	22	13.40	3.7×10^{-3} s
Improvement	93.21%	38.33%	37.29%

VI. CONCLUSION

As the common method in multi-carrier energy flow analysis, the integrated method has two problems: first, the

method will fail when energy reverses during iteration in the exceptional cases; second, the method is highly sensitive to the initial value. The fundamental causes for the two problems are revealed: the former is that the integrated method solves some equations and variables separately from the Newton-Raphson iteration; the latter is that the integrated method set part of the non-diagonal Jacobian submatrix as zero without considering the range of variables. Based on the fundamental causes, two modifications of the integrated method are made to deal with the problems: one is the simultaneous calculation of all the equations and variables in the Newton-Raphson iteration; the other is the exact calculation of the Jacobian non-diagonal submatrix considering the range of variables. Through theoretical and practical verification, the modified integrated method eliminates the failure in the exceptional cases and has less sensitivity to the initial value. Moreover, even though the modifications increase the computation burden of each iteration, the iteration times are reduced greatly and the whole computation time of the modified integrated method is decreased significantly.

REFERENCES

- [1] C. Shao, X. Wang, M. Shahidehpour, X. Wang and B. Wang, "An MILP-Based Optimal Power Flow in Multicarrier Energy Systems," *Sustainable Energy, IEEE Transactions on*, vol. 8, no. 1, pp. 239-248, Jan. 2017.
- [2] Z. Li, W. Wu, M. Shahidehpour, J. Wang and B. Zhang, "Combined Heat and Power Dispatch Considering Pipeline Energy Storage of District Heating Network," *Sustainable Energy, IEEE Transactions on*, vol. 7, no. 1, pp. 12-22, Jan. 2016.
- [3] X. Zhang, M. Shahidehpour, A. Alabdulwahab and A. Abusorrah, "Optimal Expansion Planning of Energy Hub With Multiple Energy Infrastructures," *Smart Grid, IEEE Transactions on*, vol. 6, no. 5, pp. 2302-2311, Sept. 2015.
- [4] W. Wang, D. Wang, H. Jia, Z. Chen and J. Tang, "A Decomposed Solution of Multi-energy Flow in Regional Integrated Energy Systems Considering Operational Constraints," *Energy Procedia*, Vol. 105, pp. 2335-2341, 2017.
- [5] Z. Pan, Q. Guo and H. Sun, "Interactions of district electricity and heating systems considering time-scale characteristics based on quasi-steady multi-energy flow," *Applied Energy*, Vol. 167, pp. 230-243, 2016.
- [6] X. Liu, "Combined analysis of electricity and heat networks," Ph.D. dissertation, Institute of Energy, Cardiff Univ., Cardiff, Wales, 2013.
- [7] A. Martinez-Mares and C. R. Fuerte-Esquivel, "A Unified Gas and Power Flow Analysis in Natural Gas and Electricity Coupled Networks," *Power Systems, IEEE Transactions on*, vol. 27, no. 4, pp. 2156-2166, Nov. 2012.
- [8] A. Shabanpour-Haghighi and A. R. Seifi, "An Integrated Steady-State Operation Assessment of Electrical, Natural Gas, and District Heating Networks," *Power Systems, IEEE Transactions on*, vol. 31, no. 5, pp. 3636-3647, Sept. 2016.
- [9] S. Chen, Z. Wei, G. Sun, K. W. Cheung and Y. Sun, "Multi-Linear Probabilistic Energy Flow Analysis of Integrated Electrical and Natural-Gas Systems," *Power Systems, IEEE Transactions on*, vol. 32, no. 3, pp. 1970-1979, May 2017.
- [10] X. Liu, J. Wu, N. Jenkins and A. Bagdanavicius, "Combined analysis of electricity and heat networks," *Applied Energy*, Vol. 162, pp. 1238-1250, 2016.
- [11] X. Liu, P. Mancarella and J. Wu, "A tool for integrated analysis of multi-vector district energy networks," *2015 IEEE Eindhoven PowerTech, Eindhoven*, pp. 1-6, 2015.
- [12] J. Shi, L. Wang, Y. Wang and J. Zhang, "Generalized Energy Flow Analysis Considering Electricity Gas and Heat Subsystems in Local-Area Energy Systems Integration," *Energies*, Vol. 10, pp. 514, 2016.
- [13] X. Liu and P. Mancarella, "Modelling, assessment and Sankey diagrams of integrated electricity-heat-gas networks in multi-vector district energy systems," *Applied Energy*, Vol. 167, pp. 336-352, 2016.